Phonon modes and Raman scattering in $GaAs/Ga_{1-x}Al_xAs$

Bangfen Zhu* and K. A. Chao
Department of Physics and Measurement Technology, University of Linköping, S-58183 Linköping, Sweden
(Received 7 November 1986)

The phonon modes and the Raman backscattering along the [001] direction in $GaAs/Ga_{1-x}Al_xAs$ superlattices and heterostructures have been investigated with a linear-chain model. The sample is simulated with a computer, and then exact solutions are obtained numerically. The Raman intensity is calculated with the bond-polarizability approximation. The zone folding, the disorder effect, and the quantum-well confinement have been studied in detail and compared with experiments. In particular, the controversial experimental observations over the disorder effect on the Raman $z(xx)\bar{z}$ intensity scattered by the topmost longitudinal-acoustical phonon mode is resolved.

I. INTRODUCTION

The development of molecular-beam epitaxy and metal-organic chemical-vapor deposition techniques allows the fabrication of semiconductor superlattice crystals. Let A_m/B_n represent a superlattice crystal made from alternating m layers of A semiconductor and n layers of B semiconductor. If the lattice constant of the A semiconductor is not nearly the same as the lattice constant of the B semiconductor, the strain field at the interfaces introduces additional complication to the superlattice. Here we are not interested in such strained-layer superlattices. Instead, in this paper we will study only the $GaAs/Ga_{1-x}Al_xAs$ superlattice since the lattice constant of pure GaAs and the lattice constant of pure AlAs are almost the same.

For an ideal GaAs/AlAs superlattice with alternating m layers GaAs and n layers AlAs, the superperiodicity along the direction perpendicular to the interface, say, the z axis, is $m+n$. Hence, both the electron and the phonon Brillouin zones of the pure GaAs crystal (or AlAs crystal) are folded into $m+n$ minizones along the k_z direction. This zone folding creates many novel phenomena in the superlattice. However, in this paper we will restrict ourselves to those associated to the lattice vibration.

The zone folding creates many extra phonon branches and many extra zone-center modes which may be detected by Raman scattering. The acoustical branches of both GaAs and AlAs overlap almost completely. Hence, the acoustical vibrations propagate through the entire superlattice and manifest the phenomenon of folding. On the other hand, the optical branches of GaAs and AlAs are separated in energy. Then, the GaAs (or AlAs) optical modes cannot propagate and become confined in individual GaAs (or AlAs) slab. Consequently, in GaAs/AlAs superlattice, the quantum-well confinement appears in both the electron and the phonon properties.

The quality of a superlattice is determined mainly by the sharpness of the interfaces, and the fluctuations of the layer numbers (or the thickness) of each constituent material throughout the whole superlattice. Because of the strong dependence of the lattice vibration on nearest-neighbor bonds, the phonon modes are very sensitive to imperfections of the superlattice. Thus, Raman scattering can explore the microscopic nature of structural and/or topological disorder in the GaAs/AlAs superlattice on a scale of the order of a few lattice constants. Furthermore, by doing Raman scattering on the $GaAs/Ga_{1-x}Al_xAs$ alloy superlattice, the characteristic features connected with true layering may be distinguished from the effects associated with disorder.

There has been extensive Raman investigation on both GaAs/AlAs and $GaAs/Ga_{1-x}Al_xAs$. The early report of Barker *et al.*[1] on the observation of zone folding was questioned by Merlin *et al.*,[2] who proposed an alternative explanation in terms of a phenomenological theory for the effect of layering-induced anisotropy on the frequencies of phonons. Subsequent experiments,[3–7] however, have brought strong evidence for the folding of acoustical branches and the confinement of optical phonons. Recent resonance Raman measurements with right-angle scattering[8] and with backscattering[9] also demonstrate, respectively, the confinement of optical branches in GaAs quantum-well heterostructures and in GaAs/AlAs superlattices.

The specific features related to the formation of superlattice were also reported by many authors. Narayanamurti *et al.*[10] have observed selective transmission of high-frequency phonons in $GaAs/Ga_{0.5}Al_{0.5}As$. With increasing substrate temperature, the broadening of interface widths causes a decreasing intensity of the folded acoustical modes and a frequency shift of the confined GaAs optical modes.[11] The interface vibrational modes were also detected by Raman scattering with laser energies near the confined exciton levels of the GaAs quantum wells.[12]

The disorder in superlattices may activate new Raman modes. Additional disorder-activated (DA) modes were indeed observed in the Raman spectrum of $GaAs/Ga_{1-x}Al_xAs$ but not in GaAs/AlAs. The DA LA mode appears[7,13] at the top of the LA branch around 200 cm^{-1}, and the DA TA mode has been found[5,7] in the frequency range between 50 and 100 cm^{-1}. The Raman intensities of these DA modes increase with $|0.5-x|$. Nevertheless, Barker *et al.*[1] obtained quite different conclusion regarding the effect of disorder on the LA mode at the top of the LA branch, which they called the 201-cm^{-1}

mode. In a monolayer crystal of GaAs/AlAs, they detected a strong Raman intensity due to a folded zone-center mode with frequency 201 cm^{-1}. By making the system random alloy $Ga_{0.55}Al_{0.45}As$, the Raman intensity of the 201-cm^{-1} mode gets weaker. Colvard *et al.*[7] have also seen the DA LA and the DA TA modes in GaAs/AlAs superlattice crystal of thicker GaAs slabs and AlAs slabs. With increasing temperatures the Raman peaks of both the DA LA and the DA TA become broader.

Almost all theoretical studies on the Raman spectra of GaAs/$Ga_{1-x}Al_xAs$ superlattices, quantum wells, and heterostructures are based on either the linear-chain model[1,6,14–16] or the elastic continuum model.[15,17] The elaborated calculation of Yip and Chang[18] on GaAs/AlAs, using the bond-charge model as a starting point, is difficult to be generalized to alloy superlattice GaAs/$Ga_{1-x}Al_xAs$. On the other hand, Parayanthal and Pollak have tried to fit the Raman line shape of GaAs/$Ga_{1-x}Al_xAs$ with a phenomenological spatial-correlation model with a Gaussian correlation function.[19]

In this paper we will use the linear-chain model to perform an exact numerical study on the phonon properties which are associated to the Raman scattering from the GaAs/$Ga_{1-x}Al_xAs$ superlattices. The chain will be sufficiently long such that not only the numerical results converge but also the model system is comparable in size to real samples. For the acoustical phonons, our results demonstrate a blue shift of the Raman peak positions corresponding to the zone-center modes, as the value of x increases. The controversial experimental findings on the dependence of the DA LA (or the 201 cm^{-1}) mode Raman intensity on the degree of alloying will be clarified. Finally, we will establish the correspondence between the Raman peaks and the LO modes confined in the GaAs quantum wells.

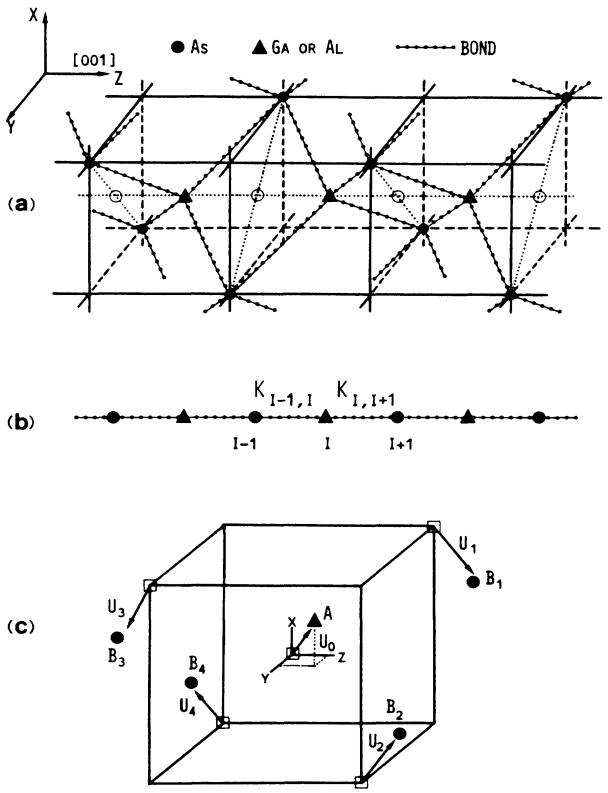

FIG. 1. The linear-chain model for the calculation of the phonon modes and the Raman intensities.

II. LATTICE VIBRATIONS

Since almost all GaAs/$Ga_{1-x}Al_xAs$ superlattice samples studied with Raman scattering were grown on an (001) oriented substrate of GaAs, the theoretical analysis on phonon modes can be much simplified. Let us first consider a lattice wave propagating in an ideal bulk crystal with its wave-vector parallel to the [001] direction. From the group theory it can be shown that the transverse vibrations and the longitudinal vibrations belong to different representation.[20] Hence, in this case the transverse- and the longitudinal-vibrational modes are decoupled. In general, the complete separation of the transverse and the longitudinal vibrations with the wave-vector parallel to [001] is also assumed in GaAs/$Ga_{1-x}Al_xAs$, provided that the aluminum atoms are uniformly distributed in the $Ga_{1-x}Al_xAs$ layers. In this paper we adopt this argument, which allows us to use the linear-chain model to study the longitudinal phonons in GaAs/$Ga_{1-x}Al_xAs$.

The model is illustrated in Fig. 1. Along the [001] direction, which is our z axis, the positions of atoms are shown in Fig. 1(a). The As atoms (indicated by solid circles) form every second (001) plane. For pure GaAs (or AlAs), between each pair of adjacent As planes there is one plane containing only Ga atoms (or Al atoms) which are marked by solid triangles. For the $Ga_{1-x}Al_xAs$ alloy, each solid triangle represents either a Ga atom or an Al atom.

For longitudinal modes with wave vectors parallel to the [001] axis, all atoms in a single (001) plane vibrate as a whole. Therefore, we project the positions of atoms on the [001] axis, as shown by (b) of Fig. 1. For a given value of x, we simulate a chain of GaAs/$Ga_{1-x}Al_xAs$ superlattice with the random-number generator of a computer. Let U_i be the displacement of the ith atom, and $K_{i,i+1}$ be the force constant between the ith and the $(i+1)$th atoms. Then, the equation of motion of the ith atom is simply

$$M_i(d^2U_i/dt^2) = -K_{i-1,i}(U_i - U_{i-1}) - K_{i,i+1}(U_i - U_{i+1}) \quad i = 1,2,\ldots,N \ , \tag{1}$$

where M_i is the mass of the ith atom. Since we know from the computer simulation the types of atoms at positions $i-1$, i, and $i+1$, the set of N coupled equations (1) can be solved numerically. With the modern computation techniques one can easily obtain the exact solution of (1) for a long chain of the order $N \simeq 10^4$.

The elastic moduli of GaAs are nearly the same as those of AlAs. Hence, in almost all existing theoretical analyses on Raman scattering from GaAs/$Ga_{1-x}Al_xAs$ superlattices, a single force constant $K_{ij}=K$ has been reasonably assumed in order to simplify the calculation. We will further normalize the phonon energy by setting $K=1$ and the mass of As $M_{As}=1$. In this energy unit the top of the longitudinal-acoustical branch has the value $(2K/M_{As})^{1/2}=\sqrt{2}$.

We use the expression $\mu[(GaAs)_n(Ga_{1-x}Al_xAs)_m]$ to represent a superlattice made of μ repeated units. In each unit there are n layers of GaAs and m layers of $Ga_{1-x}Al_xAs$. When we simulate the superlattice with a computer, in the segment $(Ga_{1-x}Al_xAs)_m$, between two As atoms the probability to have a Ga atom is $1-x$ and the probability to have an Al atom is x. Consequently, in the so-simulated segment $(Ga_{1-x}Al_xAs)_m$ the first and the mth non-As atom may not be aluminum if $x\neq 1$. In other words, the values of n and m fluctuate along the chain under the condition $n+m=$constant. We call such superlattice the *free-end* superlattice. In order to have sharp interfaces in our samples, we can eliminate the fluctuation by setting one Al atom at the first and one Al atom at the mth non-As position. To simulate the rest of the $(Ga_{1-x}Al_xAs)_m$ segment, we need to change the value of x into $(mx-2)/(m-2)$. We call such superlattice with sharp interfaces the *rigid-end* superlattice.

Figure 2 shows the calculated phonon density of states $D(E)$ for $x=0.3$, $n=m=22$, and $\mu=200$. Figure 2(a) is for a rigid-end superlattice. The acoustical branch splits into 44 minibranches as a result of the zone folding, and the GaAs optical branch reduces to 22 discrete levels in the quantum wells. The AlAs optical branch contains only well-localized modes. Similar results for the free-end superlattice are given in Fig. 2(b). We have also solved Eq. (1) for a heterostructure $(Ga_{1-x}Al_xAs)_{100}(GaAs)_{22}(Ga_{1-x}Al_xAs)_{100}$. The phonon density of states $D(E)$ is shown in Fig. 1(c). A heterostructure can be viewed as a random distribution of segments of $(GaAs)_n$ and $(AlAs)_m$ along the [001] direction with extremely large fluctuations in the values of m and n. By comparing Figs. 2(a)–2(c), we come to the conclusion that as the fluctuations in m and n increase, the loss of long-range order very effectively removes the zone-folding phenomenon. However, there remain many GaAs quantum wells of various sizes. The superposition of all discrete levels of optical phonons confined in different GaAs quantum wells forms a broad GaAs optical band. We also notice that the top of the acoustical branch (marked by an arrow) is pinned at $E=\sqrt{2}$. The measured maximum acoustical phonon energy is around 200 cm^{-1}. Consequently, the energy scale used in our calculation is 141 cm^{-1}.

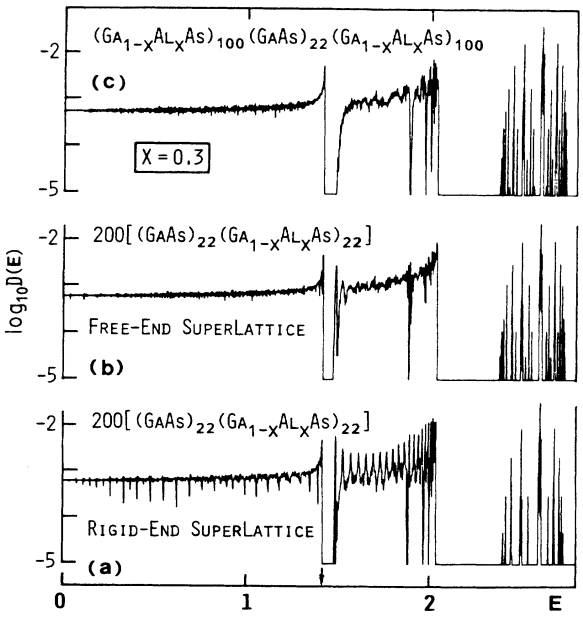

FIG. 2. The phonon density of states of superlattices and heterostructures.

In the rest of this paper we will restrict ourselves to rigid-end superlattices. The zone folding, the disorder effect, and the quantum-well confinement will be investigated separated in connection to their Raman activities.

III. RAMAN SCATTERING

The intensity of the Raman scattered light of frequency ω_s is given by the general formula[21]

$$\mathcal{I}(\omega_s)=(\omega_i^4/2\pi c^3)\sum_{\alpha,\beta,\gamma,\lambda}\hat{\eta}_\alpha\hat{\eta}_\beta\mathcal{J}_{\alpha\gamma,\beta\lambda}(\omega)\mathcal{E}_\gamma(\omega_i)\mathcal{E}^*_\lambda(\omega_i)\ , \tag{2}$$

where ω_i is the frequency of the incident light, $\hat{\eta}$ is a unit vector parallel to the electric field of the scattered light, and $\mathcal{E}(\omega_i)$ is the Fourier component of the incident electric field. The Raman tensor of frequency $\omega=\omega_i-\omega_s$ can be calculated from

$$\mathcal{J}_{\alpha\gamma,\beta\lambda}(\omega)=\int dE_i D(E_i)\sum_f \langle\Phi_i|P_{\beta\lambda}|\Phi_f\rangle\langle\Phi_f|P^*_{\alpha\gamma}|\Phi_i\rangle \times\delta(\hbar\omega-E_f+E_i)\ , \tag{3}$$

where $|\Phi_i\rangle$ and $|\Phi_f\rangle$ are the initial- and the final-phonon states with eigenenergies E_i and E_f, respectively. $P_{\alpha\gamma}$ is the transition probability tensor

$$P_{\alpha\gamma}=\sum_{\nu\neq 0}(\epsilon_\nu-\epsilon_0)^{-1}(\langle\Psi_0|M_\alpha|\Psi_\nu\rangle\langle\Psi_\nu|M_\gamma|\Psi_0\rangle + \langle\Psi_0|M_\gamma|\Psi_\nu\rangle\langle\Psi_\nu|M_\alpha|\Psi_0\rangle) \tag{4}$$

of the electric dipole moment $\mathbf{M}$ between two electronic eigenstates $|\Psi_0\rangle$ and $|\Psi_\nu\rangle$ with eigenenergies ϵ_0 and ϵ_ν, respectively.

The matrix elements and the eigenenergies in the above Eq. (4) are functions of nuclear positions $\{\mathbf{R}_i;i=1,2,\ldots,N\}$. For covalent bonding materials $P_{\alpha\gamma}$ can be

calculated with the bond-polarizability approximation.[1,6,22] In this approximation, each bond carries a bond charge which contributes to the total crystal polarizability. Let $\mathbf{r}_i$ be the equilibrium position and $\mathbf{u}_i$ the displacement of the ith atom, and $\mathbf{R}_i=\mathbf{r}_i+\mathbf{u}_i$. Then, an axially symmetric bond polarizability tensor $P_{\alpha\gamma}(\mathbf{R}_{ij})$ is associated to the bond (ij), where $\mathbf{R}_{ij}=\mathbf{R}_j-\mathbf{R}_i$. If we define $\tilde{P}(\mathbf{R}_{ij})$ the mean polarizability and $\gamma(\mathbf{R}_{ij})$ the anisotropy, we may write

$$P_{\alpha\gamma}(\mathbf{R}_{ij})=[\tilde{P}(\mathbf{R}_{ij})\underline{I}+\gamma(\mathbf{R}_{ij})(\hat{\mathbf{R}}_{ij}\hat{\mathbf{R}}_{ij}-\tfrac{1}{3}\underline{I})]_{\alpha\gamma}\ , \tag{5}$$

where $\hat{\mathbf{R}}_{ij}=\mathbf{R}_{ij}/R_{ij}$, and $\underline{I}$ is a unit tensor.

Let $\mathbf{R}_{ij}=\mathbf{r}_{ij}+\mathbf{u}_{ij}$, where $\mathbf{r}_{ij}=\mathbf{r}_j-\mathbf{r}_i$ and $\mathbf{u}_{ij}=\mathbf{u}_j-\mathbf{u}_i$. Since $u_{ij}\ll r_{ij}$, we can expand $P_{\alpha\gamma}(\mathbf{R}_{ij})$ in powers of $\mathbf{u}_{ij}$. The zeroth-order term $P_{\alpha\gamma}(\mathbf{r}_{ij})$ can be ignored since the total contribution of the zeroth order to the Raman intensity from all bonds vanishes. To the first order in $\mathbf{u}_{ij}$, we have

$$P_{\alpha\gamma}(\mathbf{R}_{ij})\simeq(\mathbf{u}_{ij}\cdot\hat{\mathbf{r}}_{ij})[\tilde{P}'(r_{ij})\underline{I}+\gamma'(r_{ij})(\hat{\mathbf{r}}_{ij}\hat{\mathbf{r}}_{ij}-\tfrac{1}{3}\underline{I})]_{\alpha\gamma}+r_{ij}^{-1}\gamma(r_{ij})[\mathbf{u}_{ij}\hat{\mathbf{r}}_{ij}+\hat{\mathbf{r}}_{ij}\mathbf{u}_{ij}-2(\mathbf{u}_{ij}\cdot\hat{\mathbf{r}}_{ij})\hat{\mathbf{r}}_{ij}\hat{\mathbf{r}}_{ij}]_{\alpha\gamma}\ , \tag{6}$$

where $\hat{\mathbf{r}}_{ij}=\mathbf{r}_{ij}/r_{ij}$ and $\tilde{P}'(R_{ij})$ and $\gamma'(r_{ij})$ are derivatives of $\tilde{P}(R_{ij})$ and $\gamma(R_{ij})$ evaluated at $u_{ij}=0$, respectively.

To calculate the Raman scattering from a superlattice structure shown in Fig. 1(a), we divide the system into groups of four bonds. Each group is illustrated in Fig. 1(c). The atom A at the center of the cube is either a Ga atom or an Al atom. Four As atoms B_1, B_2, B_3, and B_4 are at the corners. The equilibrium positions of the atoms are marked by squares. The bond polarizability tensor $\underline{P}(\mathbf{R}_{01})$ associated to the bond between atoms A and B_1 is derived as

$$\underline{P}(\mathbf{R}_{01})=\frac{1}{\sqrt{3}}(u_{01,x}+u_{02,y}+u_{03,z})\left[\tilde{P}'_A\begin{pmatrix}1&0&0\\0&1&0\\0&0&1\end{pmatrix}+\tfrac{1}{3}\gamma'_A\begin{pmatrix}0&-1&1\\-1&0&-1\\1&-1&0\end{pmatrix}\right]$$
$$+\tfrac{1}{3}\gamma_A\begin{pmatrix}2u_{01,y}-2u_{01,z}+4u_{01,x}&-u_{01,x}+u_{01,y}+2u_{01,z}&u_{01,x}+2u_{01,y}+u_{01,z}\\-u_{01,x}+u_{01,y}+2u_{01,z}&-2u_{01,x}-2u_{01,z}-4u_{01,y}&2u_{01,x}+u_{01,y}-u_{01,z}\\u_{01,x}+2u_{01,y}+u_{01,z}&2u_{01,x}+u_{01,y}-u_{01,z}&-2u_{01,x}-2u_{01,y}+4u_{01,z}\end{pmatrix}\ . \tag{7}$$

The values of γ_A, $\tilde{P}'_A$, and γ'_A are determined by the type of A atom, i.e., a Ga atom or an Al atom.

We can also calculate the bond polarizability tensor $\underline{P}(\mathbf{R}_{02})$ for the pair of atoms A and B_2. For longitudinal vibration modes, we only need the contributions from longitudinal displacements $u_{01,z}$ and $u_{02,z}$. Then, we have for longitudinal modes

$$[\underline{P}(\mathbf{R}_{01})+\underline{P}(\mathbf{R}_{02})]_L=\tfrac{1}{2}(u_{01,z}+u_{02,z})\begin{pmatrix}\alpha_{xx,A}&\alpha_{xy,A}&0\\\alpha_{xy,A}&\alpha_{xx,A}&0\\0&0&\frac{2}{\sqrt{3}}\tilde{P}'_A+\frac{8}{9}\gamma_A\end{pmatrix}\ , \tag{8}$$

where

$$\alpha_{xx,A}=\tfrac{1}{3}(2\sqrt{3}\tilde{P}'_A-\tfrac{4}{3}\gamma_A)\ , \tag{9a}$$

and

$$\alpha_{xy,A}=-\tfrac{1}{3}\left[\frac{2}{\sqrt{3}}\gamma'_A-\tfrac{4}{3}\gamma_A\right]\ . \tag{9b}$$

Similarly, from the two bonds between the atoms A and B_3, and between the atoms A and B_4, the bond polarizability tensor for longitudinal modes is

$$[\underline{P}(\mathbf{R}_{03})+\underline{P}(\mathbf{R}_{04})]_L=\tfrac{1}{2}(u_{03,z}+u_{04,z})\begin{pmatrix}-\alpha_{xx,A}&\alpha_{xy,A}&0\\\alpha_{xy,A}&-\alpha_{xx,A}&0\\0&0&\frac{2}{\sqrt{3}}\tilde{P}'_A+\frac{8}{9}\gamma_A\end{pmatrix}\ . \tag{10}$$

As we have mentioned in the preceding section, for the longitudinal vibrations with wave vectors parallel to the [001] axis, all atoms in a single (001) plane move as a whole. Hence, we have $u_{1z}=u_{2z}$ and $u_{3z}=u_{4z}$. Most Raman scattering experiments were performed with backscattering geometry. Therefore, we will study the Raman backscattering with the incoming electric field polarized along the x axis. For Raman scattering geometry $z(xx)\bar{z}$, the scattered electric field is also polarized along the x axis. In this case the Raman tensor $R_{xx}(\omega)$ is readily cal-

culated from Eqs. (3), (8), and (10) as

$$\omega R_{xx}(\omega) \equiv \mathcal{J}_{xx,xx}(\omega) \propto \left| \sum_A \alpha_{xx,A}(u_{1z} - u_{3z}) \right|^2 , \quad (11)$$

where the summation runs over all A atoms which are indicated by the solid triangles in Fig. 1. For another Raman backscattering geometry $z(xy)\bar{z}$, the scattered electric field is polarized along the y axis. The Raman tensor $R_{xy}(\omega)$ can then be expressed as

$$\omega R_{xy}(\omega) \equiv \mathcal{J}_{yx,yx}(\omega) \propto \left| \sum_A \alpha_{xy,A}(u_{1z} + u_{3z} - 2u_{0z}) \right|^2 . \quad (12)$$

IV. ZONE-FOLDING AND DISORDER EFFECT IN ACOUSTICAL BRANCH

In this section we will study the acoustical phonons and their Raman activities. For given superlattice structure generated on a computer, we solve Eq. (1) to obtain all phonon eigenenergies and eigenstates. Knowing the eigenstates, the Raman intensities R_{xx} and R_{xy} are calculated from Eqs. (11) and (12) with the values $\alpha_{xx,A}$ and $\alpha_{xy,A}$ from Barker *et al.*[1] The Raman peak at each eigenenergy is then broadened with a Gaussian of half-width 3×10^{-3}.

Let us first consider the acoustical branch of the $\mu[(\mathrm{GaAs})_n(\mathrm{AlAs})_m]$ superlattice crystal. The Raman spectra of four samples are shown in Fig. 3 with the corresponding values of $\mu(n,m)$ specified next to each spectrum. The zone-folding effect is clearly demonstrated. We should point out that if we magnify the spectra, each of the strong peaks splits into a doublet of nonequal weights. The separation of a typical doublet is about 4 cm^{-1}. The doublet structure in Raman spectrum has been observed in many experiments.[3,5–7,11] Although the measured splits of doublets are also in the range 4–6 cm^{-1}, each measured doublet has nearly equal weights in intensities.

The three samples 50(7,7), 50(5,9), and 50(4,10) have the same total number of layers $n+m=14$. The aluminum content increases from 50% in sample 50(7,7), to 64.3% in sample 50(5,9), and to 71.5% in sample 50(4,10). When the aluminum content increases, there is a blue shift of every Raman peak. This blue shift has its origin in the fact that the longitudinal-acoustical phonons of pure AlAs have higher energy than the corresponding longitudinal-acoustical phonons of pure GaAs.

The phonon mode at the top of the acoustical branch, namely, the 201-cm^{-1} mode, is Raman R_{xx} active only for samples with $n=$odd and $m=$odd, as can be seen in Fig. 3. Besides, we found that the Raman intensity of this mode is exactly the same in both samples 50(7,7) and 50(5,9). We will return to this point later with more discussion.

Now we consider the effect of disorder in alloy superlattice $\mu[(\mathrm{GaAs})_n(\mathrm{Ga}_{1-x}\mathrm{Al}_x\mathrm{As})_m]$. The Raman spectra R_{xx} and R_{xy} of the superlattice crystal 50(7,7) with $x=1$ are shown again at the bottom of Fig. 4. The middle spectra in Fig. 4 are for an alloy superlattice 50(7,7) with $x=0.3$. The Raman spectra of a random alloy $(\mathrm{Ga}_{0.7}\mathrm{Al}_{0.3}\mathrm{As})_{1400}$ are also plotted at the top of Fig. 4. The change of spectra from the completely ordered to the completely random samples indicates that the short-wavelength phonons are more sensitive to the random po-

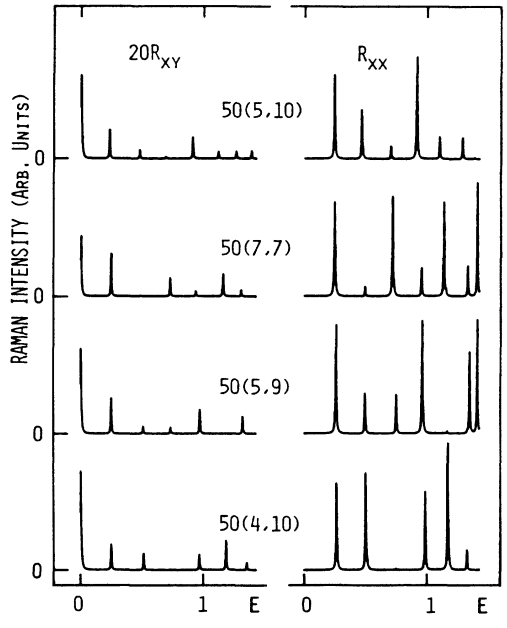

FIG. 3. Calculated Raman intensities of superlattice crystals. The numbers are values of $\mu(n,m)$ in $\mu[(\mathrm{GaAs})_n(\mathrm{AlAs})_m]$. The energy units is 141 cm^{-1}.

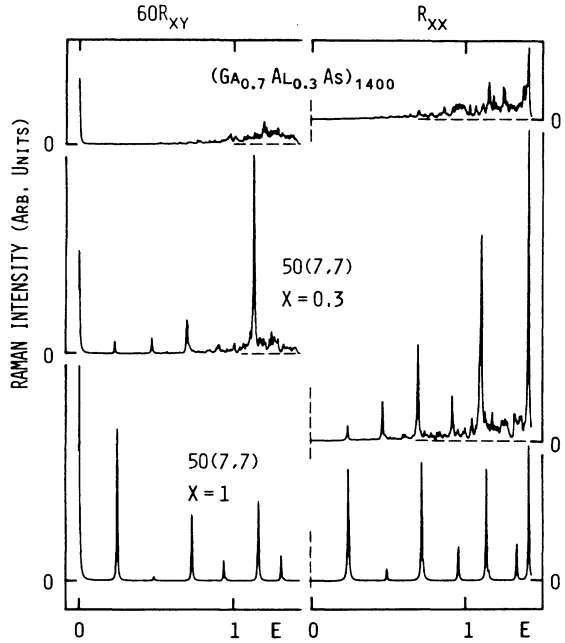

FIG. 4. Same as Fig. 3 but for alloy superlattice $\mu[(\mathrm{GaAs})_n(\mathrm{Ga}_{1-x}\mathrm{Al}_x\mathrm{As})_m]$ and random alloy.

tential, as expected.

From Fig. 4, we see that the intensity R_{xx} of the 201-cm^{-1} mode in the 50(7,7) sample indeed grows with increasing degree of disorder. In order to understand the behavior of this mode, in Fig. 5 we plot its vibration pattern in the sample $60[(GaAs)_7(Ga_{1-x}Al_xAs)_7]$. The first plot from the top is for the superlattice crystal with $x=1$, and the third plot from the top is for the alloy superlattice with $x=0.3$. In both cases the vibration amplitudes of both Ga atoms and Al atoms are too small to be seen. Therefore, these two plots show practically the vibration amplitudes of the As atoms only. In Fig. 5 we also show separately the vibration amplitudes of Ga atoms and Al atoms with a magnified scale.

The essential point in the computation of the Raman intensity R_{xx} of the 201-cm^{-1} mode is schematically illustrated in Fig. 6. Here we have segments of three different superlattice crystals $\mu[(GaAs)_n(AlAs)_m]$. The positions of the Ga atoms are marked by squares, and the positions of the Al atoms by triangles. The vertical bars represent the longitudinal displacements of the As atoms. The three samples are topologically different in structure: n is even and m is even for sample (a), n is odd and m is even for sample (b), and n is odd and m is odd for sample (c). To calculate R_{xx} from Eq. (11), let us divide the summation of A into a subsummation over all Ga atoms and a subsummation over all Al atoms. From the longitudinal displacement pattern of the As atoms shown in Fig. 5, within a finite segment of n GaAs layers or m AlAs-layers, the As-atom vibrational amplitudes are practically constant. Therefore, as shown in Fig. 6, the positive terms in the subsummation over all Ga atoms just cancel the negative terms in the same subsummation, if m is even. The same cancellation occurs in the subsummation over all Al atoms if n is even. Consequently, R_{xx} remains finite only if n is odd and m is odd, namely, the sample (c) in Fig. 6. In this nontrivial case, among the n GaAs layers (or m AlAs layers) in each GaAs (or AlAs) segment, the contributions of $n-1$ (or $m-1$) layers cancel each other. Only one layer from each segment contributes to the Raman intensity R_{xx}.

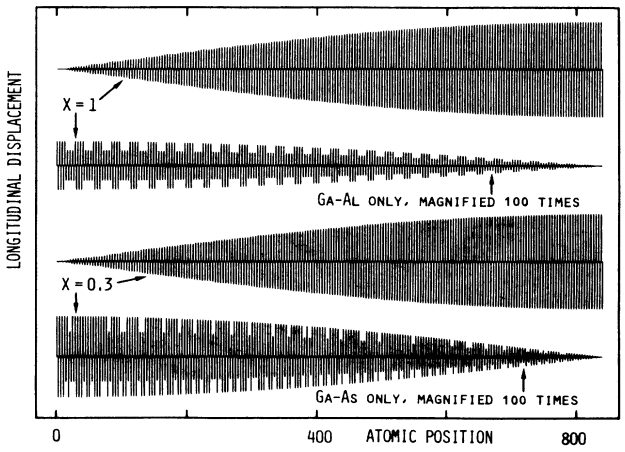

FIG. 5. The vibration pattern of the 201-cm^{-1} mode in a superlattice $60[(GaAs)_7(Ga_{1-x}Al_xAs)_7]$.

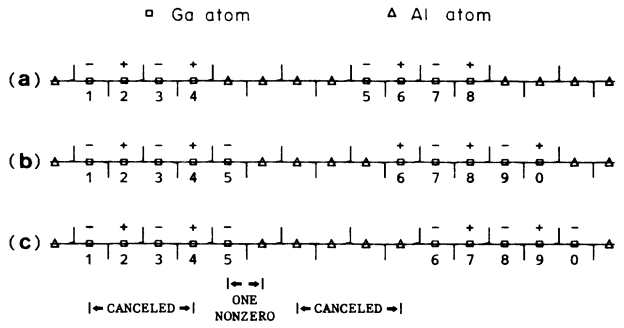

FIG. 6. A schematical illustration for the calculation of the 201-cm^{-1} mode Raman intensity R_{xx}.

In a superlattice crystal $\mu[(GaAs)_n(AlAs)_m]$, segments of ordered constituent materials (GaAs or AlAs) are separated by interfaces. Let M_L (or M_R) be the number of layers in the constituent semiconductor at the left-side (or right-side) of an interface. According to the numbers M_L and M_R being even or odd, we classify an interface as even-even, even-odd, odd-even, or odd-odd interface. From the analysis in the preceding paragraph, it is clear that only those bonds attached to the Ga atom and the Al atom at the odd-odd interface contribute to the Raman R_{xx} intensity of the 201-cm^{-1} longitudinal-acoustical mode. One such interface is marked in Fig. 6(c) as "one nonzero." The R_{xx} intensity is then proportional to the number of odd-odd interfaces per layer. For a superlattice crystal $\mu[(GaAs)_n(AlAs)_m]$ with n being odd and m being odd, there are two odd-odd interfaces per $(m+n)$ layers. This explains why in Fig. 3 the samples 50(5,10) and 50(4,10) have zero R_{xx} intensity, but the samples 50(7,7) and 50(5,9) have exactly the same R_{xx} intensity from the 201-cm^{-1} mode.

Although the above argument is for the 201-cm^{-1} mode in a superlattice crystal, it is also valid for alloy superlattices $GaAs/Ga_{1-x}Al_xAs$ and random alloys $Ga_{1-x}Al_xAs$. A given sample, ordered or random, can always be separated into segments of pure constituent semiconductors AsAs and AlAs. An interface between two adjacent segments can be even-even, even-odd, odd-even, or odd-odd. Nevertheless, only the odd-odd interfaces contributes to the 201-cm^{-1} mode Raman R_{xx} intensity. Consequently, if we start from a superlattice

TABLE I. 201-cm^{-1} mode Raman R_{xx} intensity from superlattice $50[(GaAs)_n(Ga_{1-x}Al_xAs)_m]$.

n	m	$x=1$	$x=0.5$	$x=0.3$
7	7	0.0172		0.0393
5	9	0.0172		0.0485
8	6	<0.001	0.0043	0.0030
4	10	<0.001		0.0007
10	5	<0.001		0.0022
8	7	<0.001	0.0057	0.0040
5	10	<0.001		0.0068

crystal $\mu[(GaAs)_n(AlAs)_m]$ with large values of n and m, and make it into an alloy superlattice $\mu[(GaAs)_n(Ga_{1-x}Al_xAs)_m]$, the number of odd-odd interfaces will first increase and then decrease as x changes from 1 to 0. The 201-cm^{-1} mode Raman R_{xx} intensity should behave similarly as x varies. This result agrees with the experimentally observed characteristic properties of the DA LA mode. A quantitative example is given in Table I.

On the other hand, in a monolayer superlattice crystal $n=1$ and $m=1$, there is one odd-odd interface per layer. Therefore, the 201-cm^{-1} mode has the strongest Raman R_{xx} intensity. If we change the same sample into a random alloy, the number of odd-odd interfaces per layer decreases and so the Raman intensity drops. This is what Barker *et al.*[1] have observed.

As a conclusion, the behavior of the 201-cm^{-1} mode Raman activity can not be understood unless we take into account both the zone-folding and the disorder effects.

V. CONFINED GaAs OPTICAL MODES

The confinement of GaAs optical phonons occurs in both $\mu[(GaAs)_n(Ga_{1-x}Al_xAs)]$ alloy superlattices and

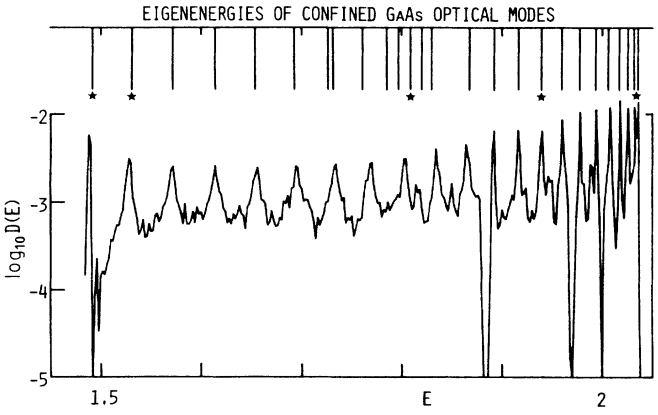

FIG. 7. Phonon density of states of confined GaAs optical modes in a superlattice (bottom) compared to the positions of the Raman peaks calculated with a heterostructure. See text for details.

$(Ga_{1-x}Al_xAs)_l(GaAs)_n(Ga_{1-x}Al_xAs)_m$ heterostructures. The longitudinal-optical phonon branch of the rigid-end superlattice $200[(GaAs)_{22}(Ga_{0.7}Al_{0.3}As)_{22}]$ was studied earlier, and its density of states was shown in Fig. 2. The

TABLE II. Longitudinal optical-phonon energies E_S confined in quantum wells in superlattice $200[(GaAs)_{22}(Ga_{0.7}Al_{0.3}As)_{22}]$, and E_H confined in quantum wells in heterostructure $(Ga_{0.7}Al_{0.3}As)_{100}(GaAs)_{22}(Ga_{0.7}Al_{0.3}As)_{100}$. E_R is the Raman peak position and R_{xx} and R_{xy} are the corresponding Raman intensities calculated with the heterostructure system. The minus integer (for example, $-n$) in each value of R_{xx} or R_{xy} indicates the power of 10 (for example, 10^{-n}).

E_S	E_H	E_R	R_{xx}	R_{xy}
1.490	1.489	1.4879	0.50(−4)	0.26(−6)
1.531	1.529	1.5202	0.10(−6)	0.13(−10)
1.573	1.570	1.5741	0.38(−4)	0.54(−6)
1.615	1.612	1.6132	0.12(−4)	0.43(−4)
		1.6150	0.35(−4)	0.21(−4)
1.656	1.652	1.6438	0.39(−4)	0.14(−7)
1.695	1.691	1.6918	0.14(−4)	0.14(−6)
		1.6980	0.35(−3)	0.12(−4)
	1.725			
1.732	1.730	1.7316	0.13(−6)	0.84(−8)
1.768	1.759	1.7639	0.13(−6)	0.12(−4)
	1.784			
	1.796			
1.801	1.808	1.8003	0.53(−6)	0.46(−5)
	1.819			
1.833	1.829	1.8329	0.51(−7)	0.54(−5)
		1.8595	0.22(−5)	0.17(−6)
1.862	1.867	1.8689	0.56(−4)	0.47(−7)
1.890	1.892	1.8906	0.86(−5)	0.13(−4)
1.915	1.916	1.9149	0.11(−4)	0.46(−5)
1.938	1.939	1.9353	0.36(−6)	0.33(−5)
		1.9403	0.30(−4)	0.15(−50)
1.958	1.959	1.9590	0.36(−5)	0.20(−5)
1.977	1.977	1.9768	0.13(−6)	0.15(−4)
1.992	1.993	1.9917	0.61(−6)	0.19(−6)
		1.9943	0.20(−4)	0.59(−7)
2.006	2.006	2.0063	0.10(−5)	0.10(−3)
2.017	2.017	2.0172	0.24(−5)	0.12(−5)
		2.0256	0.42(−7)	0.96(−3)
2.026	2.026	2.0262	0.16(−6)	0.12(−3)
2.032	2.032	2.0320	0.62(−6)	0.14(−5)
2.036	2.036	2.0357	0.24(−2)	0.28(−7)

GaAs optical branch is given again in the lower part of Fig. 7. The corresponding eigenenergies are listed in Table II under the first column E_S.

We then consider the heterostructure $(Ga_{0.7}Al_{0.3}As)_m(GaAs)_{22}(Ga_{0.7}Al_{0.3}As)_m$. For convenience, the positions of the $2M$ atoms along the chain are labeled as

$$i=-M,-M+1,\ldots,-1,0,1,\ldots,M-2,M-1\ ,$$

where $M=2m+22$. Let the As atoms occupy the odd positions

$$i=-M+1,-M+3,\ldots,-1,1,\ldots,M-3,M-1\ ,$$

and the segment $(GaAs)_{22}$ occupy the central region $i=-22,\ -21\ ,\ldots,20,\ 21$. It is important to mention that we have applied the rigid-end condition to simulate all samples. That is, at the positions $i=-24$ and 22 the atoms are aluminum. We have investigated the confined optical modes in different samples with value of m as large as 700. However, the eigenenergies and the Raman activities of the confined modes converge rapidly when the value of m increases to about 100. Hence, the results discussed here were calculated with $m=100$. The phonon density of states of this sample has been shown in Fig. 2.

Since we know all eigenstates of our heterostructure sample, we can examine these eigenmodes to find out which are localized in the central $(GaAs)_{22}$ slab. Instead of 22, we discovered 26 confined optical modes. The eigenenergies of these modes are listed in Table II under the second column E_H. In Fig. 7 these 26 eigenenergies are indicated by vertical bars above the density-of-state curve of the superlattice sample. Except for the eight eigenenergies in the region from $E=1.725$ to 1.833, we see an almost perfect match between the positions of the vertical bars and the corresponding positions of the peaks in the density-of-state curve.

The eigenfunctions $\Phi_E(i)$ of the six eigenenergies marked by stars in Fig. 7 are plotted in Fig. 8. Along the chain the quantum well is located between $i=-22$ and 21. The three high-energy modes ($E=2.036$, 2.032, and 1.939) are entirely confined in the quantum well. Since in Fig. 8 the vertical axis has logarithmic scale, the vibrations of the two low-energy modes ($E=1.489$ and 1.529) are mainly confined in the quantum well. On the other hand, the vibration of the eigenmode with energy $E=1.808$ extends over a region almost 3 times the quantum-well width. This state and a few other states are the hybridized results of the localized optical modes in the central $(GaAs)_{22}$ slab and the localized modes in adjacent $(GaAs)_l$ segments. Such hybridized modes have eigenenergies between $E=1.725$ and $E=1.833$.

The topological structures of our rigid-end heterostructure and rigid-end superlattice are entirely different. Yet the well-confined optical phonons in both samples have almost the same characteristic properties. The only common feature in the structure of these two samples is the rigid-end condition imposed on the $(GaAs)_{22}$ segment. That is, the $(GaAs)_{22}$ segment is connected to an aluminum atom at each end. Since the aluminum mass is only about 40% of the gallium mass, and since the lattice vibration is very sensitive to local defect, the termination of

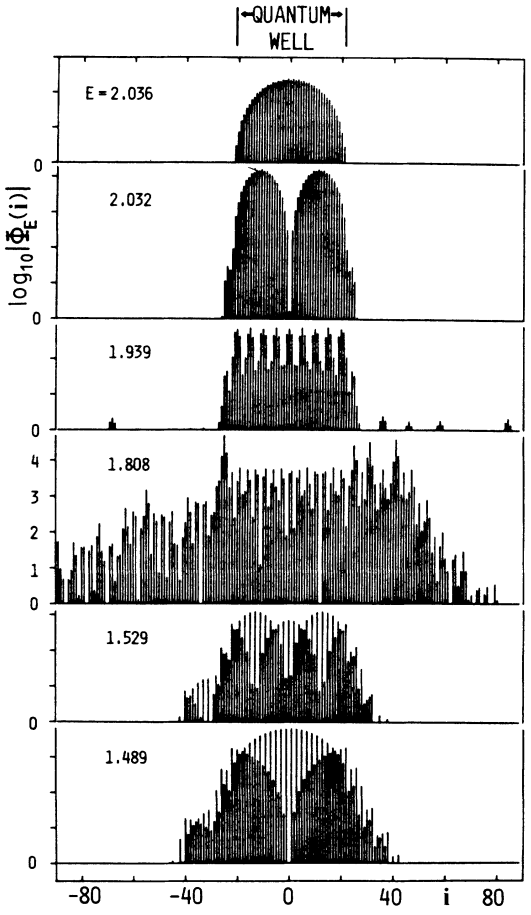

FIG. 8. Optical phonon eigenmodes confined in the quantum well in a heterostructure. E is the eigenenergy and i labels the positions of atoms along the chain.

a pure GaAs crystal by aluminum *defects* at both ends must play the crucial role in the confinement of GaAs optical phonons.

The Raman $R_{xx}(E_R)$ and $R_{xy}(E_R)$ intensities are computed with Eqs. (11) and (12) for phonon energy E_R in the GaAs longitudinal-optical branch of the $(Ga_{0.7}Al_{0.3}As)_{100}(GaAs)_{22}(Ga_{0.7}Al_{0.3}As)_{100}$ heterostructure sample. Raman intensities as weak as 10^{-10} are detected. The calculated Raman peak positions E_R and the corresponding intensities are given in Table II under the last three columns. We see a good correlation between the confined optical-phonon energies and the Raman line positions.

We have performed similar calculations on many $\mu[(GaAs)_n(Ga_{0.7}Al_{0.3}As)_m]$ superlattice samples and $(Ga_{0.7}Al_{0.3}Al)_l(GaAs)_n(Ga_{0.7}Al_{0.3}As)_l$ heterostructure samples with different values of n and m. As long as m is not very small compared to n, the result depends mainly on the value of n but not on the value of m. Consequently, the zone-folding phenomenon is irrelevant to the confinement of GaAs optical phonons in quantum wells.

Many authors have observed the longitudinal GaAs op-

tical phonons which are confined at the top of quantum wells with Raman scattering (Refs. 1, 3–9, 12, 23, and 24). However, there is no report on the detection of longitudinal GaAs optical phonons which are confined at the bottom of quantum wells. We have only found in Fig. 16 of Ref. 7 a broad maximum of Raman intensity around the Raman shift 210 cm^{-1}, measured at low temperature 2.1 K. We need more experimental data to determine whether this broad maximum is due to the optical-phonon modes confined at the bottom of quantum wells.

The good correlation between the phonon energies and the positions of Raman lines in Table II reflects the absence of Raman activities of the GaAs-like optical phonons localized in the alloy part of the sample. This is owing to the value $x=0.3$ we have used in our calculation. In the alloy part $Ga_{1-x}Al_xAs$, the probability to have a pure $(GaAs)_\nu$ segment is $(1-x)^\nu$. If x is not very small, the probability diminishes rapidly with increasing ν. In fact, we have repeated our calculation with $x<0.3$, and found no significant change of the results until x is reduced to 0.15.

To close this paper, we must point out that although the linear-chain model can explain qualitatively a reasonable amount of experimental observations, it is too crude to give quantitative agreement between the calculation and the experiment. For example, when we vary the number n in the heterostructure sample $(Ga_{0.7}Al_{0.3}As)_m(GaAs)_n(Ga_{0.7}Al_{0.3}As)_m$, and calculate the confined optical-phonon Raman R_{xy} peak positions as functions of n, only the curve of the highest Raman shift agrees well with the experimental observations.

ACKNOWLEDGMENT

This work was financially supported by the Swedish Natural Science Research Council under Grant No. NFR-FHF-3996-135.

*Permanent address: Institute of Semiconductors, Chinese Academy of Sciences, Beijing, People's Republic of China.

[1]A. S. Barker, Jr., J. L. Merz, and A. C. Gossard, Phys. Rev. B **17**, 3181 (1978).

[2]R. Merlin, C. Colvard, M. V. Klein, H. Morkoc, A. Y. Cho, and A. G. Gossard, Appl. Phys. Lett. **36**, 43 (1980).

[3]C. Colvard, R. Merlin, M. V. Klein, and A. C. Gossard, Phys. Rev. Lett. **45**, 298 (1980).

[4]C. Colvard, R. Merlin, M. V. Klein, and A. C. Gossard, J. Phys. (Paris) Colloq. **42**, C6-631 (1981).

[5]J. Sapriel, J. C. Michel, J. C. Tolédano, R. Vacher, J. Kervarec, and A. Regreny, Phys. Rev. B **28**, 2007 (1983).

[6]B. Jusserand, D. Paquet, and A. Regreny, Phys. Rev. B **30**, 6245 (1984); Superlatt. Microstruc. **1**, 61 (1985).

[7]C. Colvard, T. A. Gant, M. V. Klein, R. Merlin, R. Fischer, H. Morkoc, and A. C. Gossard, Phys. Rev. B **31**, 2080 (1985).

[8]J. E. Zucker, A. Pinczuk, D. S. Chemla, A. C. Gossard, and W. Wiegmann, Phys. Rev. Lett. **53**, 1280 (1984).

[9]A. K. Sood, J. Menéndez, M. Cardona, and K. Ploog, Phys. Rev. Lett. **53**, 2111 (1985).

[10]V. Narayanamurti, H. L. Störmer, M. A. Chin, A. C. Gossard, and W. Wiegmann, Phys. Rev. Lett. **43**, 2012 (1979).

[11]B. Jusserand, F. Alexandre, D. Paquet, and G. Le Roux, Appl. Phys. Lett. **47**, 301 (1985).

[12]A. K. Sood, J. Menéndez, M. Cardona, and K. Ploog, Phys. Rev. Lett. **54**, 2115 (1985).

[13]R. Tsu, H. Kawamura, and L. Esaki, *Proceedings of the International Conference on the Physics of Semiconductors, Warsaw, 1972* (Elsevier, Amsterdam, 1972), Vol. 2, p. 1135.

[14]R. Tsu and S. S. Jha, Appl. Phys. Lett. **20**, 1 (1972).

[15]J. Sapriel, B. Djafari-Rouhani, and L. Dobrzynski, Surf. Sci. **126**, 197 (1983).

[16]B. Djafari-Rouhani, J. Sapriel, and F. Bonnouvrier, Superlatt. Microstruc. **1**, 29 (1985).

[17]M. Babiker, J. Phys. C **19**, L339 (1986).

[18]Sung-kit Yip and Yia-Chung Chang, Phys. Rev. B **30**, 7037 (1984).

[19]P. Parayanthal and F. H. Pollak, Phys. Rev. Lett. **52**, 1822 (1984).

[20]J. L. Yarnell, J. L. Warren, R. G. Wenzel, and P. J. Dean, *Neutron Inelastic Scattering* (IAEA, Vienna, 1968), Vol. 1, p. 301.

[21]M. Born and K. Huang, *Dynamical Theory of Crystal Lattices* (Oxford University Press, London, 1954), p. 368.

[22]R. J. Bell, in *Methods in Computational Physics*, edited by B. Alder, S. Fernbach, and M. Rotenberg (Academic, New York, 1976), Vol. 15, p. 260.

[23]G. A. Sai-Halasz, A. Pinczuk, P. Y. Yu, and L. Esaki, Solid State Commun. **25**, 381 (1978); Surf. Sci. **73**, 232 (1978).

[24]J. E. Zucker, A. Pinczuk, D. S. Chemla, A. Gossard, and W. Wiegmann, Phys. Rev. B **29**, 7065 (1984).